Taylor & Francis
Taylor & Francis Group

Automatika

Journal for Control, Measurement, Electronics, Computing and Communications

ISSN: (Print) (Online) Journal homepage: https://www.tandfonline.com/loi/taut20

Robust adaptive sliding mode control of a MEMS tunable capacitor based on dead-zone method

Ehsan Ranjbar, Mostafa Yaghubi & Amir Abolfazl Suratgar

To cite this article: Ehsan Ranjbar, Mostafa Yaghubi & Amir Abolfazl Suratgar (2020) Robust adaptive sliding mode control of a MEMS tunable capacitor based on dead-zone method, Automatika, 61:4, 587-601, DOI: 10.1080/00051144.2020.1806011

To link to this article: https://doi.org/10.1080/00051144.2020.1806011

Published online: 24 Aug 2020.

AUTOMATIKA
2020, VOL. 61, NO. 4, 587–601
https://doi.org/10.1080/00051144.2020.1806011

REGULAR PAPER

OPEN ACCESS Check for updates

Robust adaptive sliding mode control of a MEMS tunable capacitor based on dead-zone method

Ehsan Ranjbar [a,b], Mostafa Yaghubi[b] and Amir Abolfazl Suratgar[a,b]

[a]MEMS Dynamics & Control Research Group, Industrial Control Lab, Department of Electrical Engineering, Amirkabir University of Technology, Tehran, Iran; [b]Department of Electrical Engineering, Amirkabir University of Technology, Tehran, Iran

ABSTRACT

Uncertainty in parameters of a tunable Micro Electro Mechanical System (MEMS) capacitor, as the main component of AC Voltage Reference Source (VRS), is significant to obtain a precise output voltage unaffected by disturbance and noise. Although attempts are done to craft the capacitor with desired physical specification and improve accuracy of parameters, parametric uncertainties transpire in manufacturing due to micro-machining shortcomings. First off, this paper remarks design of a Robust Adaptive Sliding Mode Controller (RASMC) and its application for the MEMS AC VRS for the first time so that it can produce a stable precise regulated output at presence of uncertainties and disturbance. Secondly, it makes a comparison between the proposed novel controller and our previously designed ASMC. The comparison reassures one of robustness at exacerbating conditions in the tunable capacitor dynamics. The novelty is employment of the dead zone-based ASMC to manage parametric uncertainty and disturbance in the MEMS tunable capacitor. It also contributes to adaptive sliding mode control of the dynamics with stiffness and damping coefficients, which are non-slowly-varying time-dependent parameters, approaching dead-zone method. Uncertainty in the plate mass besides bounded time-variant uncertainty in stiffness and damping are considered. These restrictions were not deemed in the previous design.

ARTICLE HISTORY
Received 27 May 2020
Accepted 20 July 2020

KEYWORDS
Bounded time-variant parameter variation; dead-zone; MEMS; robust adaptive sliding mode control; tunable capacitor

1. Introduction

Rudimentary principals of AC and DC Micro Electro Mechanical System (MEMS)-based Voltage Reference Source (VRS) were firstly provided by [1]. They suggested a micro parallel-moving plate capacitor which is utilized in an elementary circuit to produce a fixed voltage. The capacitor specification which is established upon great mechanical stability of single crystalline silicon brings about accurate output voltage between its plates. Moreover, low production charge and tininess make these voltage sources exclusive apparatus for electronic functions. Other researchers began working on the VRS to ameliorate their preciseness. There are some papers which concentrate on micromachining procedures of MEMS tunable capacitors [2–7] because of the importance of the MEMS tunable capacitor fabrication specification as the major component of MEMS VRS. The dominant common target in these pieces is proposal and fabrication of novel schemes of tiny tunable capacitors as well as quality enhancement in the final fabricated MEMS VRS.

Exploiting tunable capacitor in MEMS VRS is interconnected with pull-in point. It is a critical point and shows a distinctive quality which originates from electromechanical coupling between the applied electrostatic force and the spring reaction coercion. As it is illustrated in Figure 1(a,b), the electro static force will increase if the electric charge is more accumulated over the capacitive plates. Consequently, the movable plate of the capacitor is guided towards the settled plate gently, until the spring force could not tolerate the electrostatic force any more. This point is entitled as the pull-in point. Adjacent to this point, the voltage variation between the capacitor plates is proportional to the square of deflection in the moving plate. Thus, the VRS will provide a regulated output working about the pull-in point, and the MEMS VRS is finally operated close to the pull-in point of its MEMS tunable capacitor. Based on [8], mechanical stress and electrical charge over dielectric layer logically bring about instability about the pull-in point. They affirmed that AC voltage exploitation, instead of DC voltage, discounts the charge aggregation over the dielectric layer. Utilizing AC voltage input yielded in innovation of MEMS AC VRS. In our article, the MEMS AC VRS operation is deemed.

CONTACT Ehsan Ranjbar en.ranjbar.eeng@gmail.com MEMS Dynamics & Control Research Group, Industrial Control Lab, Department of Electrical Engineering, Amirkabir University of Technology, Tehran, Iran; Department of Electrical Engineering, Amirkabir University of Technology, Tehran, Iran

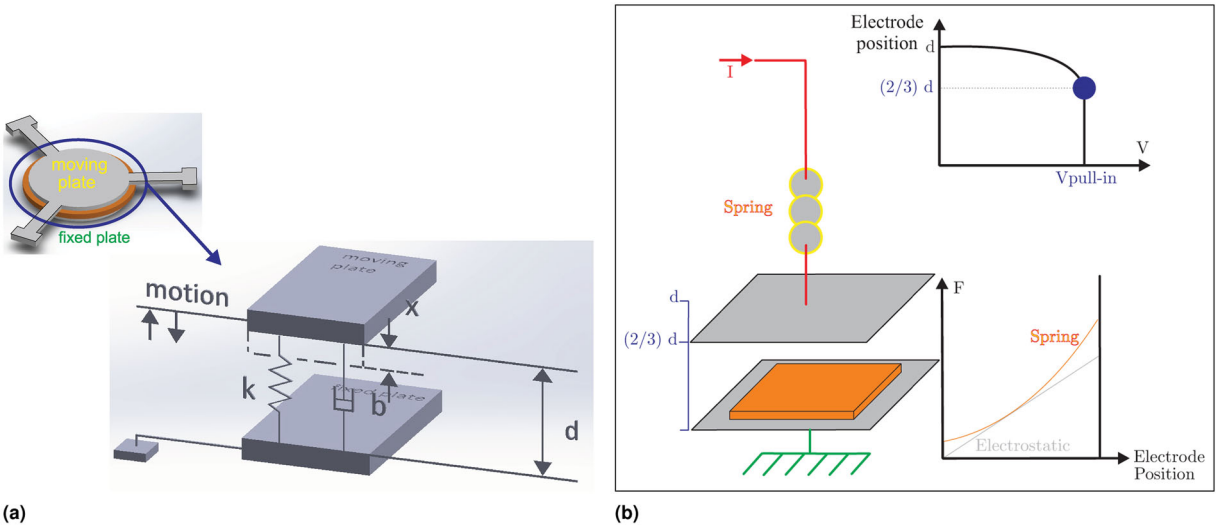

Figure 1. (a) MEMS tunable capacitor and its model. (b) Pull-in point is the point in which movable electrode gets to one third of its primary distance to stationary electrode [24].

Today, the modern micro-fabrication tech assists us to fabricate the MEMS tunable capacitors greatly with precise dimensions and geometries and less mechanical stress. Nonetheless, application of controllers to the MEMS VRS is integral since it affects the lifelong stability and preciseness of the reference voltage. It is not blowing it out of proportion that applying efficient control algorithms to robots and other mechatronic systems to yield error decrease and improved performance is a remarkable challenge for researchers of control engineering science and technology [9]. Numerous algorithms are also focused on MEMS dynamics and control issues such as [10–12]. The corresponding application field is vast and sometimes astonishing! Furthermore, adaptive and robust control techniques remain at the focus of researchers' awareness on the ground of defects in modelling of MEMS and parametric uncertainties in their manufacturing procedures [13–18]. Adaptive sliding mode control is one of the most popular methods in MEMS or other mechatronic systems dynamics and control research since it copes with parameter uncertainty and disturbance rejection simultaneously [19–22].

A state space model is introduced in [23] to exploit different control solutions in practice for MEMS tunable capacitors. The controller is used to move the capacitor movable plate towards the pull-in point and maintain it there while the capacitor parameters, such as spring stiffness, vary with time progression. When the system parameters are considered steady, the target is achieved employing an elementary pole-placement state feedback controller. Nonetheless, it emerges problematic while it is known that unavoidable uncertainties exist in the capacitor parameters. Typically, the accurate spring stiffness value might not be known. The problem grows more challenging when noisy electrical measurements, mechanical noise and time-variant parameters are considered to tackle the real situation.

This paper is concerned with design of a Robust Adaptive Sliding Mode Controller (RASMC) based on dead-zone technique to cope with certain types of parametric uncertainties in the MEMS tunable capacitor system dynamics. It is employed in such a way that the movable plate in the capacitor structure could perfectly track a non-destructive moving trajectory to get placed at the pull-in point, regarding benefits of the pull-in operational zone. It should be mentioned that the displacement trajectory of the movable plate with overshoots or very fast rise-time might corrupt the microstructure of the device. The first noticeable contribution of this article is consideration of possible uncertainty in the movable plate mass which is innately an invariable uncertainty. The second novel improvement in this paper is contemplation of a distinct class of time-variable bounded uncertainty in stiffness and damping factors and coping with it on the ground of dead-zone on-off switching of adaptation mechanism. The results are so satisfactory that one may approve of considerable robustness in the dead-zone-based RASMC in comparison to our previous conventional adaptive sliding mode controller (ASMC) application in [24] and the ASMC design in [25]. It should be stated that stiffness and damping coefficients could alter as the local environmental conditions, like temperature, get changed. The mechanical noise, vibration harmonics and cross-talk may appear to affect and change damping and stiffness coefficients. It should be reminded that all of the three parameter estimation errors, associated with mass, stiffness and damping factors, remain bounded in simulation reassuring us of mathematically proven system stability.

Introducing dead zones and saturation functions in SMC in this paper is not novel. For instance, they were introduced and utilized in [26]. Actually, it is worthwhile being mentioned that the novelties in this paper can be explicitly stated and summarized as following:

(1) This article exploits the dead-zone-based adaptive sliding mode control for the MEMS voltage reference application for the first time.
(2) In previous works, they have assumed that the parametric uncertainty in the dynamics of the tunable capacitor is so that the stiffness and damping are either unknown or vary slowly relative to time. However, we have changed the presumption; the variation of the whole term of the stiffness and damping coefficients are not slow and they are quite time-dependent. The stiffness and damping factor may show an unexpected behaviour during the time of operation. Previous works on control of the capacitive plates such as [10,13,27–31] assume that the parameters are unknown constants or vary so slowly, i.e. the time-derivative of the parameters are approximately considered zero.
(3) Unlike many other works such as [32–37], which have been concerned with tracking a sinusoidal displacement trajectory for the displacement of the MEMS movable capacitive plate, this paper addresses displacement control of the movable capacitive plate, regulating its motion about a fixed position.
(4) This article deems uncertainty in the movable plate mass which has not been considered in previous works such as [24,29,30,38,39].

The paper is organized as follows: The operation principals of the MEMS tunable capacitor and its model is reviewed in Section 2. The controller design and mathematics are presented afterwards in Section 3. Subsequently, simulation results are given in Section 4. Two final sections, Sections 5 and 6, provide the article conclusion and future discussion, respectively.

2. Overview of operating principles

A tunable capacitor is mainly comprised of an unmovable and a movable plate. In our article, one of the ordinary tunable capacitors, displayed on Figure 1(a,b), is discussed. It is a MEMS parallel plate tunable capacitor and includes a movable plate which changes the interplate gap. The demanding concern, which is addressed in this article, is improving characteristics of tracking performance of the electrically charge-accumulated plate in the tunable capacitor, regarding existence of parameter uncertainty and disturbance. The plate barely gets displaced and it would not consequently get retained in the designed pull-in point [24]. It is speculated that the streamlining presumptions in modelling could be one origin of parameter uncertainty in stiffness factor in its suspension system. Other sources could be assigned to depletion of desiderated mechanical characteristics because of ageing and variation of working status which yields in parameter uncertainty. Unfortunately, deficiencies in manufacturing process could be another origin of minor uncertainty in major parameters such as plate mass, stiffness and damping factors. By and large, design and application of a control system which would handle parameter uncertainty is beneficial to deal with and spend one's focus.

In a MEMS tunable capacitor, the capacitance in Farad (F) is given by Equation (1) which is modulated by the gap;

$$C = \epsilon A / (d - x). \tag{1}$$

The parameters in Equation (1), $\epsilon = 8.85 \times 10^{-12}$ (F/m), A (m^2), d (m) and x (m), respectively, typify the medium permittivity, the electrode area, the initial gap between plates and the movable plate deviation. An AC current in Amperes (A), which is given by Equation (2), actuates the capacitor;

$$I = I_m \sin(\omega t). \tag{2}$$

Electrostatic force, F_E (N), attracts electrodes towards each other while spring force, given by kx, tries to prevent plates from getting close to each other. These two forces are equalized via Equation (3) considering Figure 1(a) [40]. The following equation describes this balance [41];

$$F_E = \left| -\frac{\partial E_I}{\partial x} \right| = \frac{I_m^2 \cos^2(\omega t)}{2\epsilon A \omega^2} = kx + b\frac{\mathrm{d}x}{\mathrm{d}t} + m\frac{\mathrm{d}^2 x}{\mathrm{d}t^2}. \tag{3}$$

The variables and parameters in Equation (3), F_E (N), E_I (N/C), x (m), k (N/m), m (Kg) and b (Ns/m), are, respectively, the electrostatic force produced by the AC current, the electrostatic energy, plate distance, spring constant, movable electrode mass and damping factor due to the existing gas between the plates. The actuation current frequency, $\omega/2\pi$ (rad/s), is almost presumed to be greater than the mechanical resonance frequency described by $\omega_0/2\pi = \sqrt{k/m}/2\pi$ (rad/s). Furthermore, the movable plate movement damps when position stability is reached. The damping factor is associated with the element gas damping. The mechanical quality factor defined for the moving plate capacitor, called Q, could be controlled, tuning the gas pressure within the element compartment;

$$Q = 1/2\zeta. \tag{4}$$

Disregarding the slide film damping due to consideration of the plate movement limitation, b represents squeeze film damping. Nevertheless, this impact is physically handled by some special fabrication precautions. Analysing quantitatively, the gas compressibility

requires to be considered. These careful actions are mentioned in [24,41]. The movable electrode position is nearly fixed during sinusoidal variations in the AC current and the electrostatic force. Actually, the force in Equation (3) could be superseded by the electrostatic force mean value. This replacement brings about Equation (5). Notably, $\omega = 2\pi/T$ and $\ddot{x}$ as well as $\dot{x}$ are nearly zero about the pull-in operation point at the steady state.

$$\begin{aligned}\bar{F}_E &= \frac{2}{T}\int_0^{\frac{T}{2}} \frac{I_m^2\cos^2(\omega t)}{2\epsilon A\omega^2}\mathrm{d}t \\ &= \frac{1}{\pi}\int_0^{\pi} \frac{I_m^2(1+\cos(2\alpha))}{4\epsilon A\omega^2}\mathrm{d}\alpha = \frac{I_{RMS}^2}{2\epsilon A\omega^2\pi} = kx\end{aligned} \tag{5}$$

The electrostatic force over the movable plate could be also estimated via Equation (6).

$$\bar{F}_E = \left|-\frac{\partial E_V}{\partial x}\right| = \frac{\epsilon A V_{RMS}^2}{2(d-x)^2} = kx \tag{6}$$

V_{RMS} symbolizes the AC voltage root mean square (RMS) between the plates and E_V stands for the electrostatic energy. Regarding x in terms of I_{RMS} from Equation (5) and replacing x in Equation (6) with the latter yield result in Equation (7) which states V_{RMS} in terms of I_{RMS} [23].

$$V_{RMS} = \frac{d}{\epsilon A\omega}I_{RMS} - \frac{1}{2k\epsilon^2A^2\omega^3}I_{RMS}^3 \tag{7}$$

Taking derivative of V_{RMS} with respect to I_{RMS} results in

$$\frac{\partial V_{RMS}}{\partial I_{RMS}} = \frac{d}{\epsilon A\omega} - \frac{3}{2k\epsilon^2A^2\omega^3}I_{RMS}^2. \tag{8}$$

The value of I_{RMS}^{max} is obtained equalizing Equation (8) to zero. It is equivalent to $\sqrt{2kd\epsilon A\omega^2/3}$. Replacing I_{RMS} in Equation (7) with I_{RMS}^{max} results in V_{RMS}^{max} entitled as the reference or pull-in voltage;

$$V_{RMS}^{\max} = \sqrt{8kd^2/27C_0} = \sqrt{8kd^3/27\epsilon A}. \tag{9}$$

x is attained by Equation (10) contemplating Equations (5) and (6) as well as considering the obtained maximum V_{RMS}^{max} and its reciprocal I_{RMS}^{max} [23].

$$x = d/3 \tag{10}$$

The main operating point in the MEMS tunable capacitors turns to be the pull-in point. As a result, tiny variations in the input current about the pull-in point and its impact on the output voltage ought to be notified more carefully. Exploiting $I_{RMS} + \Delta I$ instead of I_{RMS} in Equation (7) yields in Equation (11);

$$\Delta V = \frac{d\Delta I}{\epsilon A\omega} - \frac{(\Delta I^3 + 3I_{RMS}^{\max\,2}\Delta I + 3I_{RMS}^{\max}\Delta I^2)}{2k\epsilon^2A^2\omega^3}. \tag{11}$$

Equation (12) is obtained dividing Equation (11) by V_{RMS}^{max}.

$$\frac{\Delta V_{RMS}}{V_{RMS}^{\max}} = -\frac{3}{2}\left(\frac{\Delta I}{I_{RMS}^{\max}}\right)^2 - \frac{1}{2}\left(\frac{\Delta I}{I_{RMS}^{\max}}\right)^3 \approx -\frac{3}{2}\left(\frac{\Delta I}{I_{RMS}^{\max}}\right)^2 \tag{12}$$

Regarding Equation (12), it could be stated that the voltage variations in the pull-in point is nearly proportionate to the square of the current alterations. Therefore, tiny alterations in the input current with regard to the pull-in current cause a tiny variation in the pull-in voltage. It promotes the idea of utilization of the tunable capacitor as the main component in a voltage reference circuitry. Presuming the actuation frequency to be much greater than the mechanical resonance frequency, the electrostatic force in Equation (3) should be replaced with the electrostatic force mean value. It yields Equation (13);

$$\bar{F}_E = \frac{I_{RMS}^2}{2\epsilon A\omega^2\pi} = u = m\ddot{x}(t) + b\dot{x}(t) + kx(t). \tag{13}$$

The disturbance and parameter uncertainties are assumed to emerge in the following format in the model;

$$(m+\Delta m)\,\ddot{x} + (b+\Delta b)\,\dot{x} + (k+\Delta k)\,x = u + d_D, \tag{14}$$

where Δm is a time-invariant uncertainty in the mass, and Δb as well as Δk are, respectively, bounded time-variant uncertainties in the damping and stiffness coefficients. Additionally, d_D is bounded matched disturbance. Our goal will be design of a controller to make the movable capacitor track the following reference model so that it could be placed at the pull-in point with minimum damage to its cantilever micro-mechanical structure. This target should be obtained during transient trajectory distance travel while the system is subjected to the described exacerbated uncertain and disturbing condition. The reference model is described by Equation (15);

$$\ddot{x}_m + a_m\dot{x}_m + b_m x_m = c_m r(t). \tag{15}$$

In this equation, a_m and b_m are considered in such a way that the reference model gets stable. Those and c_m are also the tuning constants for adjusting the transient and steady-state response of the reference model.

3. Controller design

Regarding Equations (13) or (14), one may consider a more general model such as Equation (17) to tackle the

controller design problem, while taking into account Equation (16). Note that the state variable vector is defined by the following equation:

$$X = \left[x\dot{x}\ldots x^{(n-1)}\right]^T, \tag{16}$$

while the corresponding n-degree system dynamics would be assumed to be presented by Equation (17);

$$hx^{(n)} + \sum_{i=1}^{n}\left[a_i + a_{iv}(t)\right] g_i\left(X,t\right) = u. \tag{17}$$

In the above equation, g_i are nonlinear bounded functions of time and states. In addition, $h>0$ and a_i are known factors which vary so slowly while $a_{iv}(t)$ are indefinite time-dependant coefficients whose known upper bounds are $C_i(t)$;

$$|a_{iv}(t)| \le C_i(t). \tag{18}$$

Before design of the controller, some mathematical prerequisites are demonstrated. Firstly,

$$\mathrm{Sat}\left(\frac{s}{\varepsilon}\right) = \begin{cases} 1 & \frac{s}{\varepsilon} \ge 1 \\ \frac{s}{\varepsilon} & -1 \le \frac{s}{\varepsilon} < 1 \\ -1 & \frac{s}{\varepsilon} < -1 \end{cases} \tag{19}$$

and consequently

$$\varepsilon\mathrm{Sat}\left(\frac{s}{\varepsilon}\right) = \begin{cases} \varepsilon & s \ge \varepsilon \\ s & -\varepsilon \le s < \varepsilon \\ -\varepsilon & s < -\varepsilon \end{cases}. \tag{20}$$

s_ε is correspondingly defined in the following way;

$$s_\varepsilon = s - \varepsilon\,\mathrm{Sat}(s/\varepsilon). \tag{21}$$

Therefore,

$$s_\varepsilon = s - \varepsilon\,\mathrm{Sat}(s/\varepsilon) = \begin{cases} s-\varepsilon & \frac{s}{\varepsilon} \ge 1 \\ 0 & -1 \le \frac{s}{\varepsilon} < 1 \\ s+\varepsilon & \frac{s}{\varepsilon} < -1 \end{cases}, \tag{22}$$

and consequently

$$\dot{s}_\varepsilon = \begin{cases} \dot{s} & s > \varepsilon \\ 0 & -\varepsilon < s < \varepsilon \\ \dot{s} & s < -\varepsilon \end{cases}. \tag{23}$$

Note that

$$\dot{s}_\varepsilon \ne \dot{s}. \tag{24}$$

On the other hand,

$$s_\varepsilon \times \dot{s}_\varepsilon = \begin{cases} s-\varepsilon & s \ge \varepsilon \\ 0 & -\varepsilon \le s < \varepsilon \\ s+\varepsilon & s < -\varepsilon \end{cases} \times \begin{cases} \dot{s} & s > \varepsilon \\ 0 & -\varepsilon < s < \varepsilon \\ \dot{s} & s < -\varepsilon \end{cases}$$

$$= \begin{cases} s\dot{s} - \varepsilon\dot{s} & s \ge \varepsilon \\ 0 & -\varepsilon \le s < \varepsilon \\ s\dot{s} + \varepsilon\dot{s} & s < -\varepsilon \end{cases}$$

$$= \begin{cases} s-\varepsilon & s \ge \varepsilon \\ 0 & -\varepsilon \le s < \varepsilon \\ s+\varepsilon & s < -\varepsilon \end{cases} \times \dot{s} = s_\varepsilon\dot{s}.$$

Hence,

$$s_\varepsilon\dot{s}_\varepsilon = s_\varepsilon\dot{s}. \tag{25}$$

Equation (25) is the first mathematical prerequisite mentioned before. Secondly, another prerequisite equation will be of use next;

$$s_\varepsilon \times \mathrm{Sat}\left(\frac{s}{\varepsilon}\right) = \begin{cases} s-\varepsilon & s \ge \varepsilon \\ 0 & -\varepsilon \le s < \varepsilon \\ s+\varepsilon & s < -\varepsilon \end{cases}$$

$$\times \begin{cases} 1 & s \ge \varepsilon \\ \frac{s}{\varepsilon} & -\varepsilon \le s < \varepsilon \\ -1 & s < -\varepsilon \end{cases}$$

$$= \begin{cases} s-\varepsilon & s \ge \varepsilon \\ 0 & -\varepsilon \le s < \varepsilon \\ -(s+\varepsilon) & s < -\varepsilon \end{cases} = |s_\varepsilon| \Rightarrow$$

$$s_\varepsilon\mathrm{Sat}\left(s/\varepsilon\right) = |s_\varepsilon|. \tag{26}$$

Regarding the robust and the sliding mode controller design in [42], we would have

$$s\left(t\right) = \left(\mathrm{d}/\mathrm{d}t + \lambda\right)^{n-1}\tilde{x}, \tag{27}$$

which means

$$s = \tilde{x}^{(n-1)} + \lambda_{n-2}\tilde{x}^{(n-2)} + \cdots + \lambda_1\dot{\tilde{x}} + \lambda_0\tilde{x}. \tag{28}$$

The time-derivative of the sliding surface could be restated as the following:

$$\dot{s} = \tilde{x}^{(n)} + \lambda_{n-2}\tilde{x}^{(n-1)} + \cdots + \lambda_1\ddot{\tilde{x}} + \lambda_0\dot{\tilde{x}} \tag{29}$$

or

$$\dot{s} = x^{(n)} - x_m^{(n)} + \lambda_{n-2}\tilde{x}^{(n-1)} + \cdots + \lambda_1\ddot{\tilde{x}} + \lambda_0\dot{\tilde{x}}. \tag{30}$$

Defining the equivalent control law (u^* or u_{eq}) as $u_{eq}(t) = u_{fd}(t)$ by the following equation

$$u_{fd}(t) = x_m^{(n)} - \lambda_{n-2}\tilde{x}^{(n-1)} - \cdots - \lambda_1\ddot{\tilde{x}} - \lambda_0\dot{\tilde{x}}, \tag{31}$$

the time-derivative of the sliding surface will be

$$\dot{s} = x^{(n)} - u_{fd}(t). \tag{32}$$

Regarding the plant dynamics and Equation (32),

$$\dot{s} = \frac{1}{h}u - \frac{1}{h}\sum_{i=1}^{n} a_i g_i - \frac{1}{h}\sum_{i=1}^{n} a_{iv}(t) g_i - u_{fd}(t). \quad (33)$$

Having the time-derivative of the sliding surface get equal to zero, the first-assumed control law, $\hat{u}$, has to partially be constructed at least by two terms;

$$\hat{u} = \sum_{i=1}^{n} \hat{a}_i g_i + \hat{h} u_{fd}. \quad (34)$$

It should be brought into one's mind that our total approach is trying to make $\dot{s}$ equal to zero. Consequently, we should notice that one term is neglected in Equation (34). It is $\sum_{i=1}^{n} a_{iv}(t) g_i$ and has been crossed out of Equation (34) since $a_{iv}(t)$ shall not be estimated. Therefore, we tackle the problem via designing the sliding mode controller approaching adoption of another control law solution;

$$u = \sum_{i=1}^{n} \hat{a}_i g_i + \hat{h} u_{fd} - k_c s. \quad (35)$$

The term, $k_c s (k_c > 0)$, is embedded to compensate for the controversial term of $\sum_{i=1}^{n} a_{iv}(t) g_i$. Considering Equation (21), the control law would change into

$$u = \sum_{i=1}^{n} \hat{a}_i g_i + \hat{h} u_{fd} - k_c s_\varepsilon - k_c \varepsilon \mathrm{Sat}\left(\frac{s}{\varepsilon}\right) \quad (36)$$

where

$$k_c = \eta + k' \sum_{i=1}^{n} C_i(t)|g_i| \ (\eta > 0,\ k' > 0) \quad (37)$$

or

$$k_c = D + \eta + k' \sum_{i=1}^{n} C_i(t)|g_i| \ (D \geq \sup\|d_D(t)\|) \quad (38)$$

k' is a positive constant which shall be defined later, while η is used as a positive tuning constant. In addition, D is the supremum of the matched disturbance. Take notice that Equation (38) is deemed whenever the disturbance entitled $d_D(t)$ is taken into account supplanting u with $u + d_D$. Now, the Lyapunov candidate function is considered by

$$V\left(s_\varepsilon, \tilde{h}, \tilde{a}_i\right) = h s_\varepsilon^2 + \frac{1}{\gamma_0}\tilde{h}^2 + \sum_{i=1}^{n} \frac{1}{\gamma_i}\tilde{a}_i^2 \quad (39)$$

where $\gamma_0 > 0$ and $\gamma_i > 0$ are desirable constants. $\tilde{h}$ and $\tilde{a}_i$ are parameter estimation errors;

$$\tilde{h} = \hat{h} - h, \quad (40)$$

$$\tilde{a}_i = \hat{a}_i - a_i. \quad (41)$$

The time-derivative of the Lyapunov candidate function gets calculated as the following:

$$\dot{V} = 2 h s_\varepsilon \dot{s}_\varepsilon + \frac{2}{\gamma_0}\tilde{h}\dot{\tilde{h}} + \sum_{i=1}^{n} \frac{2}{\gamma_i}\tilde{a}_i \dot{\tilde{a}}_i. \quad (42)$$

Regarding Equations (25) and (33), the term, $s_\varepsilon \dot{s}_\varepsilon$, could be presented in other way;

$$\begin{aligned} s_\varepsilon \dot{s}_\varepsilon &= s_\varepsilon \dot{s} \\ &= s_\varepsilon \left(\frac{1}{h}u - \frac{1}{h}\sum_{i=1}^{n} a_i g_i - \frac{1}{h}\sum_{i=1}^{n} a_{iv}(t) g_i - u_{fd}(t)\right) \end{aligned} \quad (43)$$

Considering Equation (36) as the control law to be applied to the system,

$$\begin{aligned} s_\varepsilon \dot{s} = s_\varepsilon \Bigg(&\frac{1}{h}\sum_{i=1}^{n} \hat{a}_i g_i + \frac{\hat{h}}{h} u_{fd} - \frac{k_c}{h} s_\varepsilon - \frac{k_c \varepsilon}{h} \mathrm{Sat}\left(\frac{s}{\varepsilon}\right) \\ &- \frac{1}{h}\sum_{i=1}^{n} a_i g_i - \frac{1}{h}\sum_{i=1}^{n} a_{iv}(t) g_i - u_{fd}\Bigg) \Rightarrow \\ s_\varepsilon \dot{s} = s_\varepsilon \Bigg(&\frac{1}{h}\sum_{i=1}^{n} \left(\hat{a}_i - a_i\right) g_i + \frac{\hat{h}}{h} u_{fd} - \frac{k_c}{h} s_\varepsilon \\ &- \frac{k_c \varepsilon}{h} \mathrm{Sat}\left(\frac{s}{\varepsilon}\right) - \frac{1}{h}\sum_{i=1}^{n} a_{iv}(t) g_i - u_{fd}\Bigg) \end{aligned} \quad (44)$$

Using Equation (44) and notifying very slow variation of the parameters, a_i and h, $\dot{V}$ is re-calculated;

$$\begin{aligned} \dot{V} = 2 h s_\varepsilon \Bigg(&\frac{1}{h}\sum_{i=1}^{n} \left(\hat{a}_i - a_i\right) g_i + \frac{\hat{h}}{h} u_{fd} - \frac{k_c}{h} s_\varepsilon \\ &- \frac{k_c \varepsilon}{h} \mathrm{Sat}\left(\frac{s}{\varepsilon}\right) - \frac{1}{h}\sum_{i=1}^{n} a_{iv} g_i - u_{fd}\Bigg) \\ &+ \frac{2}{\gamma_0}\left(\hat{h} - h\right)\dot{\hat{h}} + \sum_{i=1}^{n} \frac{2}{\gamma_i}\left(\hat{a}_i - a_i\right)\dot{\hat{a}}_i \end{aligned} \quad (45)$$

Consideration of Equation (26) leads $\dot{V}$ to get much more simplified next;

$$\begin{aligned} \dot{V} = &\sum_{i=1}^{n} 2 s_\varepsilon g_i \left(\hat{a}_i - a_i\right) + 2 s_\varepsilon \hat{h} u_{fd} \\ &- 2 k_c s_\varepsilon^2 - 2 s_\varepsilon k_c \varepsilon \mathrm{Sat}\left(\frac{s}{\varepsilon}\right) \\ &- \sum_{i=1}^{n} 2 s_\varepsilon a_{iv} g_i - 2 h s_\varepsilon u_{fd} + \frac{2}{\gamma_0}\left(\hat{h} - h\right)\dot{\hat{h}} \\ &+ \sum_{i=1}^{n} \frac{2}{\gamma_i}\left(\hat{a}_i - a_i\right)\dot{\hat{a}}_i \Rightarrow \end{aligned}$$

$$\dot{V} = \sum_{i=1}^{n} \left(2s_\varepsilon g_i + \frac{2}{\gamma_i}\dot{\hat{a}}_i\right)\left(\hat{a}_i - a_i\right) + \left(2s_\varepsilon u_{fd} + \frac{2}{\gamma_0}\dot{\hat{h}}\right)\left(\hat{h} - h\right) - \sum_{i=1}^{n} 2s_\varepsilon a_{iv}(t)g_i - 2k_c s_\varepsilon^2 - 2k_c\varepsilon\, s_\varepsilon \mathrm{Sat}\left(\frac{s}{\varepsilon}\right), \tag{46}$$

and, with regard to Equation (26), $\dot{V}$ will finally get equal to

$$\dot{V} = \sum_{i=1}^{n} \left(2s_\varepsilon g_i + \frac{2}{\gamma_i}\dot{\hat{a}}_i\right)\left(\hat{a}_i - a_i\right) + \left(2s_\varepsilon u_{fd} + \frac{2}{\gamma_0}\dot{\hat{h}}\right)\left(\hat{h} - h\right) - \sum_{i=1}^{n} 2s_\varepsilon a_{iv}(t)g_i - 2k_c s_\varepsilon^2 - 2k_c\varepsilon\,|s_\varepsilon|\,. \tag{47}$$

Adopting parameters's update law by the following equations,

$$\dot{\hat{h}} = -\gamma_0 s_\varepsilon u_{fd}(t) \tag{48}$$

and

$$\dot{\hat{a}}_i = -\gamma_i s_\varepsilon g_i\,(X,t)\,, \tag{49}$$

the time-derivative of the Lyapunov candidate function gets equal to

$$\dot{V} = -2k_c s_\varepsilon^2 - 2k_c\varepsilon\,|s_\varepsilon| - \sum_{i=1}^{n} 2s_\varepsilon a_{iv}(t)g_i. \tag{50}$$

As it is seen in Equation (51), $\dot{V}$ is comprised of three main parts:

$$\dot{V} = -\underbrace{2k_c s_\varepsilon^2}_{>0} - \underbrace{2k_c\varepsilon|s_\varepsilon|}_{} - \underbrace{2s_\varepsilon \sum_{i=1}^{n} a_{iv}(t)g_i}_{}\,. \tag{51}$$

Assuring the negative-definiteness of V, the second and third terms in Equation (51) deserves of being dealt with. Regarding either Equation (37) or even Equation (38),

$$2k_c\varepsilon|s_\varepsilon| = 2\eta\varepsilon|s_\varepsilon| + 2\varepsilon|s_\varepsilon|k'\sum_{i=1}^{n} C_i(t)|g_i|. \tag{52}$$

Considering Equations (51) and (52),

$$\dot{V} = -2k_c s_\varepsilon^2 - 2\eta\varepsilon|s_\varepsilon| - 2\varepsilon|s_\varepsilon|k'\sum_{i=1}^{n} C_i|g_i| - 2s_\varepsilon\sum_{i=1}^{n} a_{iv}g_i. \tag{53}$$

Adopting $k' = \frac{1}{\varepsilon}$, the time-derivative equals to

$$\dot{V} = -2k_c s_\varepsilon^2 - 2\eta\varepsilon|s_\varepsilon| - 2|s_\varepsilon|\sum_{i=1}^{n} C_i|g_i| - 2s_\varepsilon\sum_{i=1}^{n} a_{iv}g_i. \tag{54}$$

The following term, A, is a positive term regarding the initial assumptions;

$$A = 2|s_\varepsilon|\sum_{i=1}^{n} C_i(t)|g_i| + 2s_\varepsilon\sum_{i=1}^{n} a_{iv}(t)g_i \geq 0. \tag{55}$$

The reason is that

$$\begin{aligned} C_i(t) \geq |a_{iv}(t)| &\rightarrow C_i(t)|g_i| \geq |a_{iv}(t)||g_i| \geq a_{iv}(t)g_i \\ &\rightarrow 2|s_\varepsilon|\sum_{i=1}^{n} C_i(t)|g_i| \geq 2s_\varepsilon\sum_{i=1}^{n} a_{iv}(t)g_i \\ &\rightarrow 2|s_\varepsilon|\sum_{i=1}^{n} C_i(t)|g_i| - 2s_\varepsilon\sum_{i=1}^{n} a_{iv}(t)g_i \geq 0, \end{aligned} \tag{56}$$

and consequently,

$$\underbrace{2|s_\varepsilon|\sum_{i=1}^{n} C_i|g_i| + 2s_\varepsilon\sum_{i=1}^{n} a_{iv}g_i}_{A} \geq 2|s_\varepsilon|\sum_{i=1}^{n} C_i|g_i| - 2s_\varepsilon\sum_{i=1}^{n} a_{iv}g_i \geq 0.$$

Putting them all together, $\dot{V}$ is restated:

$$\dot{V} = -\underbrace{2k_c s_\varepsilon^2}_{>0} - \underbrace{2\eta\varepsilon|s_\varepsilon|}_{>0} - \underbrace{A}_{>0} \leq 0 \tag{57}$$

Therefore, the system is stable and all the parameter estimation errors as well as tracking ones are absolutely bounded. More importantly, s_ε emerge bounded, and in mathematical terms;

$$s_\varepsilon \in L_\infty, \tag{58}$$

$$\tilde{h} \in L_\infty, \tag{59}$$

and

$$\tilde{a}_i \in L_\infty. \tag{60}$$

It is quite obvious that

$$\dot{V} \leq -2k_c s_\varepsilon^2 \leq -k_c s_\varepsilon^2 \leq 0, \tag{61}$$

relying on Equation (57). Integrating over Equation (61), $\dot{V} \leq -k_c s_\varepsilon^2$, shall be exploited in order to demonstrate

$s_\varepsilon \in L_2$. It yields either Equation (62) or (63);

$$V(t) - V(0) \leq -\int_0^t k_c s_\varepsilon^2 \mathrm{d}\tau \leq 0, \tag{62}$$

$$V(0) - V(t) \geq \int_0^t k_c s_\varepsilon^2 \mathrm{d}\tau \geq 0. \tag{63}$$

This means

$$V(t) \leq V(0). \tag{64}$$

Consequently, $V(t)$ is decreasing regarding $\dot{V} < 0$. On the other hand, $V(t)$ is positive definite and this leads $\dot{V}$ to be lower-bounded as well as upper-bounded. Explicitly, all that results in boundedness of the following integral;

$$\int_0^t k_c s_\varepsilon^2 \mathrm{d}\tau < \infty \tag{65}$$

since

$$0 \leq \int_0^t k_c s_\varepsilon^2 \mathrm{d}\tau \leq V(0) - V(t). \tag{66}$$

Developing more, Equation (65) legitimately turns to be like this;

$$\left[\int_0^t |s_\varepsilon(\tau)|^2 \mathrm{d}\tau\right]^{\frac{1}{2}} < \infty. \tag{67}$$

Equation (67) holds true for $\forall t \geq 0$ so

$$\left[\int_0^\infty |s_\varepsilon(\tau)|^2 \mathrm{d}\tau\right]^{\frac{1}{2}} < \infty \Rightarrow s_\varepsilon(t) \in L_2. \tag{68}$$

It could be alleged that $\sup_{t\geq 0} \|s_\varepsilon(t)\| < \infty$ regarding Equation (58). However, from other standing point, one may claim that the reason is if $\sup_{t\geq 0} \|s_\varepsilon(t)\|$ is unbounded, then the positive amount of integral, $[\int_0^\infty |s_\varepsilon(\tau)|^2 \mathrm{d}\tau]^{\frac{1}{2}}$ would be unbounded which is in contradiction with the proven result in Equation (67). Hence,

$$\sup_{t\geq 0} \|s_\varepsilon(t)\| < \infty \Rightarrow s_\varepsilon(t) \in L_\infty. \tag{69}$$

Definition in Equation (20) states that $\varepsilon \mathrm{Sat}(s/\varepsilon) = \begin{cases} \varepsilon & s \geq \varepsilon \\ s & -\varepsilon \leq s < \varepsilon \\ -\varepsilon & s < -\varepsilon \end{cases}$ resulting in

$$\varepsilon \mathrm{Sat}(s/\varepsilon) \in L_\infty. \tag{70}$$

Regarding Equations (20) and (69) (or (58)),

$$\left.\begin{matrix} \varepsilon \mathrm{Sat}\left(\frac{s}{\varepsilon}\right) \in L_\infty \\ s_\varepsilon(t) \in L_\infty \end{matrix}\right\} \xrightarrow{s_\varepsilon = s - \varepsilon \mathrm{Sat}\left(\frac{s}{\varepsilon}\right)} s(t) \in L_\infty. \tag{71}$$

Putting the system dynamics, the control law stated by Equations (31) and (36) all together, will result in error dynamical equation;

$$\left.\begin{matrix} hx^{(n)} + \sum_{i=1}^n [a_i + a_{iv}] g_i = u \\ u = \sum_{i=1}^n \hat{a}_i g_i + \hat{h} u_{fd} - k_c s - k_c \varepsilon \mathrm{Sat}\left(\frac{s}{\varepsilon}\right) \\ u_{fd}(t) = x_m^{(n)} - \lambda_{n-2}\tilde{x}^{(n-1)} - \cdots - \lambda_1 \ddot{\tilde{x}} - \lambda_0 \dot{\tilde{x}} \end{matrix}\right\} \xrightarrow{\hat{h} = \tilde{h} + h}$$

$$hx^{(n)} + \sum_{i=1}^n a_i g_i + \sum_{i=1}^n a_{iv} g_i$$

$$= \sum_{i=1}^n \hat{a}_i g_i + h u_{fd} + \tilde{h} u_{fd} - k_c s - k_c \varepsilon \mathrm{Sat}\left(\frac{s}{\varepsilon}\right)$$

$$\Rightarrow h\left(x^{(n)} - u_{fd}\right) + k_c s = \sum_{i=1}^n \left(\tilde{a}_i - a_{iv}\right) g_i$$

$$+ \tilde{h} u_{fd} - k_c \varepsilon \mathrm{Sat}\left(\frac{s}{\varepsilon}\right). \tag{72}$$

Regarding Equation (32),

$$h\dot{s} + k_c s = \sum_{i=1}^n \tilde{a}_i g_i - \sum_{i=1}^n a_{iv} g_i + \tilde{h} u_{fd} - k_c \varepsilon \mathrm{Sat}\left(\frac{s}{\varepsilon}\right). \tag{73}$$

$\dot{V} \leq 0$ and it brings about boundedness of $\tilde{h}$ and $\tilde{a}_i$. Note that

$$\Delta(s) = s^{n-1} + \lambda_{n-2} s^{n-2} + \cdots + \lambda_1 s + \lambda_0 \tag{74}$$

is a Hurwitz characteristic equation. Taking this into account, considering Equation (71) and definition of s by Equation (28) as well as definition of u_{fd} by Equation (31), it is concluded that $u_{fd}(t)$ gets bounded ($u_{fd} \in L_\infty$). Relying on the assumption of Equation (18) as well as Equation (73) and all the latter results, one may reassure that

$$\dot{s}(t) \in L_\infty. \tag{75}$$

If the equations of (25), (69) and (75) are deemed side by side, Equation (76) will be demonstrated;

$$\left.\begin{matrix} s_\varepsilon(t) \in L_\infty \\ \dot{s}(t) \in L_\infty \end{matrix}\right\} \xrightarrow{s_\varepsilon \dot{s}_\varepsilon = s_\varepsilon \dot{s}} \dot{s}_\varepsilon \in L_\infty. \tag{76}$$

Exploiting equations of (69), (76) and (68) as integral assumptions for Barbalet's Lemma, the zero-convergence of $s_\varepsilon(t)$ is guaranteed [42];

$$\left.\begin{matrix} s_\varepsilon(t) \in L_2, \\ s_\varepsilon(t) \in L_\infty, \dot{s}_\varepsilon(t) \in L_\infty \end{matrix}\right\} \xrightarrow{\lim_{t\to\infty} s_\varepsilon(t) = 0.} \tag{77}$$

Remembering either Equation (21) or (22) as the definition of $s_\varepsilon(t)$, s will vary between $-\varepsilon$ and $+\varepsilon$. For more clarification, one may envision the diagram of variation of s_ε with respect to s. This means

$$|s(t)| \leq \varepsilon \tag{78}$$

According to [42] as well as regarding to the following sliding surface definition,

$$s(t) = \left(\frac{\mathrm{d}}{\mathrm{d}t} + \lambda\right)^{(n-1)} \tilde{x}(t), \left(\tilde{x} = \hat{x} - x \text{ and } \lambda > 0\right), \tag{79}$$

it is concluded that

- the equation of $s(t) = 0$ is a time-dependant superplane where the tracking error of $\tilde{x}$ converge to Ω_ε;

$$\Omega_\varepsilon = \left\{ \tilde{X} \in \mathrm{IR}^n || \tilde{x}_i | \leq 2^{(i-1)} \lambda^{(i-n)} \varepsilon,\ i = 1, \ldots, n \right\}, \tag{80}$$

- if $\tilde{X}(0) \neq 0$ and $|s(t)| \leq \varepsilon$, then $\tilde{X}(t)$ converges to Ω_ε with the time-constant of τ [42];

$$\tau = (n-1)/\lambda. \tag{81}$$

Remarking Equations (48), (49) and (22) (or (21)), the parameter update laws of the system change to the following ones:

$$\dot{\hat{h}} = \begin{cases} -\gamma_0 (s - \varepsilon) u_{fd}(t) & s \geq \varepsilon \\ 0 & -\varepsilon \leq s < \varepsilon : \text{ dead zone} \\ -\gamma_0 (s + \varepsilon) u_{fd}(t) & s < -\varepsilon \end{cases} \tag{82}$$

$$\dot{\hat{a}}_i = \begin{cases} -\gamma_i (s - \varepsilon) u_{fd}(t) & s \geq \varepsilon \\ 0 & -\varepsilon \leq s < \varepsilon : \text{ dead zone} \\ -\gamma_i (s + \varepsilon) u_{fd}(t) & s < -\varepsilon \end{cases} \tag{83}$$

This means the adaptation mechanism gets off when the tracking error grows small ($-\varepsilon < s < \varepsilon$). Dead zone length, Δ_d, is equal to

$$\Delta_d = \varepsilon - (-\varepsilon) = 2\varepsilon. \tag{84}$$

Conceptually, the dead zone technique is reliant on the notification which reminds one that small tracking errors, mostly comprised of noise and disturbance, shake hand with chattering phenomena resulting in more devastating noisy trajectories. That is why the adaptation mechanism is put off while the tracking error is diminishing. Even though the possibility of small disturbances leading to instability is quite undesirable, it does not mean that adaptive control is impractical. A number of techniques for modifying the adaptation law are available to avoid the parameter drift problem [43]. The most straightforward technique, which regularly gets utilized, is the dead-zone method because of its plainness and efficiency. The whole story which could be put into a nutshell is supplanting the adaptation law

$$\dot{\hat{a}}_t = -\gamma \nu_t e_t \tag{85}$$

with

$$\dot{\hat{a}}_t = \begin{cases} -\gamma \nu_t e_t & |e_t| > \Delta_d \\ 0 & |e_t| < \Delta_d \end{cases} \tag{86}$$

where Δ_d is the dead-zone time-length [42].

Equation (86) is presented just to demonstrate that our strategy on adoption of the control law by Equation (36) leads to the adaptation laws in Equations (82) and (83) which their structure is quite similar to what has been mentioned in [42]. This adaptation mechanism does not guarantee complete zero-convergence of the error but one has the option to reduce the error via modulating Δ_d. It could be considered as a research prospective to design a better adaptation law that makes the adapted coefficients approach zero as a continuous function. It is also worthwhile elaborating and stating that total control system can be shortly described by Equations (36), (82), and (83) as the control law and the parameters update law, respectively.

In the previous ASMC design in [24], the sliding surface was deemed as

$$s(t) = \dot{e} + \lambda e, \tag{87}$$

where λ is a positive constant. The Lyapunov candidate function was suggested to be

$$V(s, \tilde{p}) = \frac{1}{2} s^2 + \frac{1}{2} \tilde{p}^T \Gamma^{-1} \tilde{p} \tag{88}$$

where $\Gamma_{2\times 2}$ is a symmetric positive definite matrix. First off, stabilizing the system, the following control law served to be

$$u = u_{lun} + W\hat{p} - a_m \dot{x} - b_m x_m + c_m r - \lambda(\dot{x} - \dot{x}_m) \tag{89}$$

where u_{lun} is given by

$$u_{lun} = -\eta_{12} \tanh(s). \tag{90}$$

In this equation, λ is a positive tuning constant, whereas a_m, b_m and c_m are constants for stability guarantee as well as adjustment of transient and steady-state response of the desired trajectory (x_m) - as introduced in the reference model of Equation (15). They are specified by the pull-in point. Additionally, η_{12} is a positive constant which is defined regarding lumped uncertainty norm. Note that lumped uncertainty is

$$l_{un} = d - \Delta b \dot{x} - \Delta k x. \tag{91}$$

Secondly, the parameters update law come along with Equations (89) and (90) to fulfill the whole system stability guarantee [24];

$$\dot{\hat{p}} = -\Gamma W^T s. \tag{92}$$

It is worthwhile notifying that the switching control effort, $u_{lun} = -\eta_{12} \operatorname{sgn}(s)$ in Equation (90), is the major source of reinforced disturbance rejection mechanism. Loosening chattering effect, other smooth transient switching functions such as $u_{lun} = -\eta_{12} \operatorname{sat}(s)$ or $u_{lun} = -\eta_{12} \tanh(s)$, which is used in the ASMC simulation, are exploited in the previous designed ASMC.

It should be clarified that we are not concerned with making a comparison between different switching functions such as sat(.), sgn(.) or tanh(.). The main

comparison which we are going to address is juxtaposition of the previously suggested ASMC and the currently proposed design of RASMC. Both are ASMCs but the latter takes advantage of the dead-zone-based adaptation laws to overcome fast variation of the parameters, including stiffness and damping coefficients, in the system dynamics. In the next section, it will be verified that the current proposed RASMC is really robust in comparison with the previous ASMC design in drive and operation of the MEMS tunable capacitor.

4. Simulation results

Simulation is done utilizing parameter values of Table 1. It is carried out using MATLAB Simulink software version R2015a. The total control sketch of an ASMC is displayed on Figure 2 as well. It includes four major parts: Desired Trajectory Generator (the model reference), Sliding Surface Generator, Parameter Update Law or the estimation block, and Control Law generation block. The distinction between block diagrams of the ASMC and our proposed dead-zone-based RASMC is in the content inside three latter mentioned blocks, suggesting no difference in wiring blocks of our RASMC. The simulation scheme of the proposed dead-zone-based RASMC is depicted on Figure 3 accompanied by the corresponding explanatory Table 2 below, which has come to clarify what inside each block is!

A constant disturbance about 1 mN is imposed on the system. There is an uncertainty as much as 95% of the nominal value in the moveable plate mass;

$$m_r = 0.95m_n. \tag{93}$$

m_r and m_n are, respectively, real and nominal values of the plate mass. Not only are the stiffness and damping factors subjected to the same 95% uncertainty factor, but also they are prone to a noisy time-variant non-biased random signal with a 1% perturbation around the nominal value entitled v_n. In mathematical words, introducing k_r, k_n, b_r and b_n as the notation for the real and nominal values of the stiffness and damping factors in the moveable plate dynamics, the assumptions come as follows;

$$k_r = 0.95k_n + k_n \times v_n \tag{94}$$

and

$$b_r = 0.95b_n + b_n \times v_n, \tag{95}$$

where perturbation signal of v_n is depicted by the following equation:

$$v_n = 0.01 \times 2 \times (rand(1) - 0.5)\,. \tag{96}$$

Note that $rand(1)$ is the function producing random real values between 0 and 1. Consequently, v_n will be a random signal between -0.01 and $+0.01$. As it could be easily seen, the situation is similar to the assumptions and theory discussed in Section 3. Typically and more importantly, there are likewise two kinds of uncertainties in the system dynamics: one time-invariant and two bounded time-variant uncertainties. Values of m_r, $0.95b_n$ and $0.95k_n$, respectively, stand for h, $a_1(t)$ and $a_2(t)$ in Equation (17). Additionally, terms of b_nv_n and k_nv_n are correspondingly $a_{1v}(t)$ and $a_{2v}(t)$. Similarly, a matched uncertainty is taken into account at the plant input either. It is also worthwhile being notified that g_1 and g_2, nonlinear bounded functions, are, respectively, $\dot{x}$ and x. The upper bounds for the time-variant parts of uncertainties in damping and stiffness coefficients, C_1 and C_2, are, respectively, equal to $0.01b_n$ and $0.01k_n$. Simulation parameters for the controller are set as the following: $\lambda_0 = 10^4$, $\varepsilon = 10^5$, $\eta = 10$, and $\gamma_0 = \gamma_1 = \gamma_2 = 100$. Reference model parameters are considered as $a_m = 10^4$, $b_m = 2.5 \times 10^7$ and $c_m = 2.5 \times 10^7$ with zero initial conditions. Initial values for three estimators are considered 90% of the nominal values of the parameters.

All the dead-zone-based RASMC simulation results are presented on Figure 5(a,b,e). They persuade one to accept the new control system performance, RASMC, as a terrific outcome since the ultimate goal, which is

Table 1. Main parameters of the tunable capacitor of the MEMS AC VRS used in the simulations [3,5,24].

Parameter	Real value	Parameter	Real value
m	1.11×10^{-7} Kg	k	2338 N/m
b	0.01 Ns/m	d	2 μm

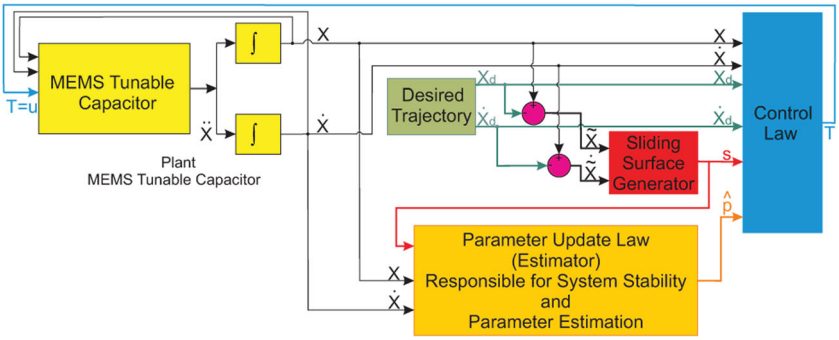

Figure 2. General scheme of an adaptive sliding mode controller.

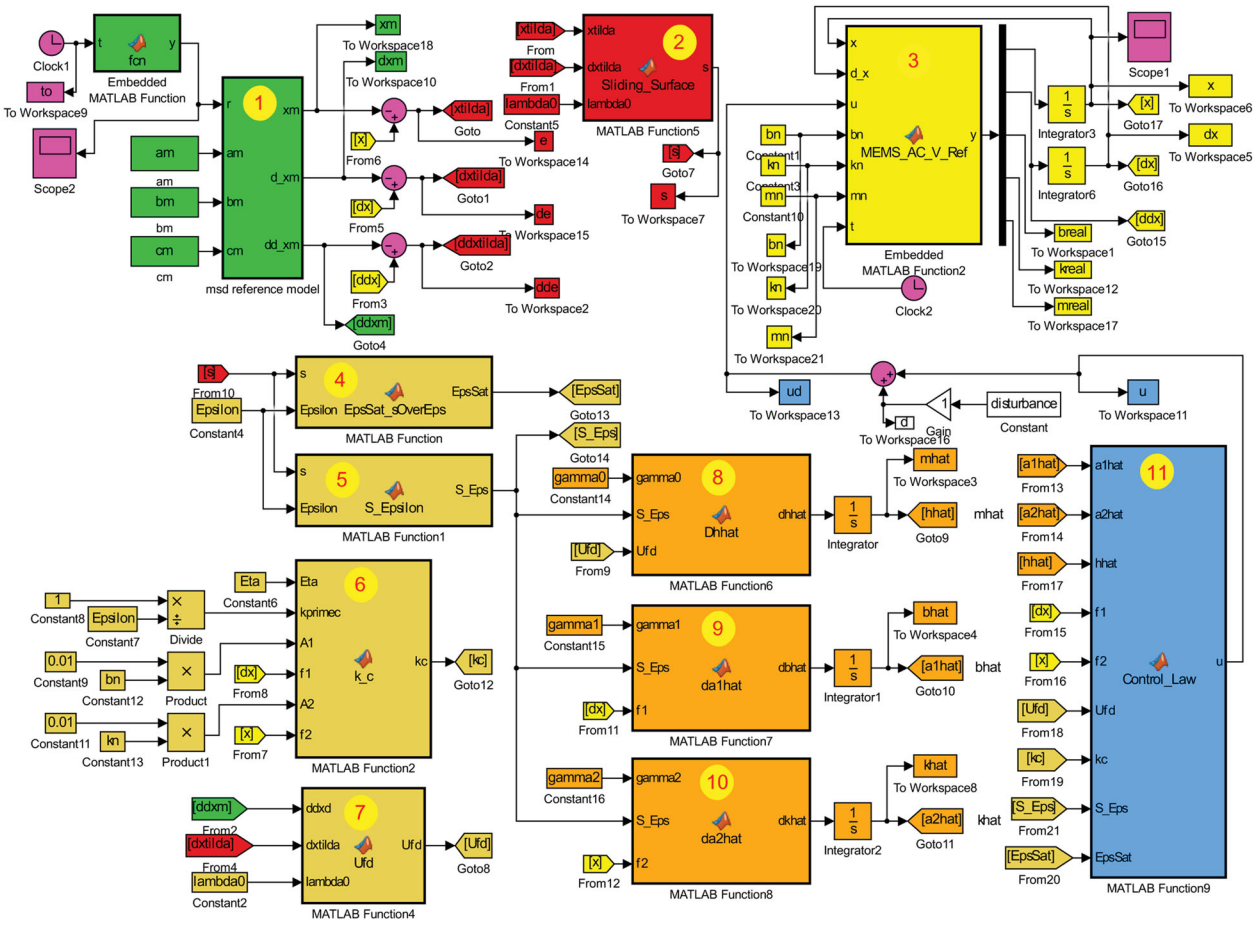

Figure 3. Simulation scheme of the RASMC design based on dead-zone method.

Table 2. Simulation blocks of the dead-zone-based RASMC and their corresponding implementation equations.

Block No.	Equation No.	Block No.	Equation No.	Block No.	Equation No.	Block No.	Equation No.	Block No.	Equation No.
1	(15)	2	(28)	3	(13)	4	(20)	5	(22)
6	(37) or (38)	7	(31)	8	(48)	9	(49)	10 11	(49) and (36)

perfect tracking of the desired trajectory, is obtained accurately! It is carried out in such a way that placement of the moveable plate at the pull-in point with a non-destructive transient trajectory is achieved in spite of the existing time-variant uncertainty in the stiffness and damping, the time-invariant uncertainty in the plate mass as well as the matched disturbance. As it is seen on Figure 5(a), the plate displacement is exactly 0.667 (μm) away from its initial distance. The red and blue curves, on the top plot of Figure 5(a), are correspondingly the desired and real trajectories of the moveable plate displacement entitled $x_m(t)$ and $x(t)$. The blue and red curves, displayed in two other plots below on Figure 5(a) are the total applied control effort and disturbance imposed on the system. The green ones on these plots are the lonesome control effort values versus the red curves of the disturbance. On Figure 5(e), we are trying to display dynamics of parameter convergence. The blue, red and green curves are, respectively, real, estimated and the nominal values of the parameters. All estimated values of the plant parameters, including the coefficients of the damping and stiffness as well as the plate mass, have remained bounded which promotes mathematically proven system stability in Section section.DesAdapCon.

The simulation scheme of the old ASMC design is given on Figure 4. Table 3 presents a guideline on the contents of the blocks shown on Figure 4 which are originally equations from (87) to (92). Results out of simulating the old ASMC design are displayed on Figure 5(c,d,f). The red and blue curves, on the top plot of Figure 5(c), are, respectively, the desired and real trajectories symbolized as $x_m(t)$ and $x(t)$. The blue curve displayed in other plot below, on Figure 5(c), is the total applied control effort at the ASMC system. Figure 5(f) intends to describe parameter convergence. The blue, red and green curves are correspondingly the estimated, real and nominal values of the parameters. All the estimated parameters of the plant dynamics, encompassing coefficients of damping and stiffness as well as plate mass, have turned bounded which bolsters up system stability. It is clear and conclusive that the time-invariant uncertainty in moveable plate mass as well as time-variant stiffness and damping

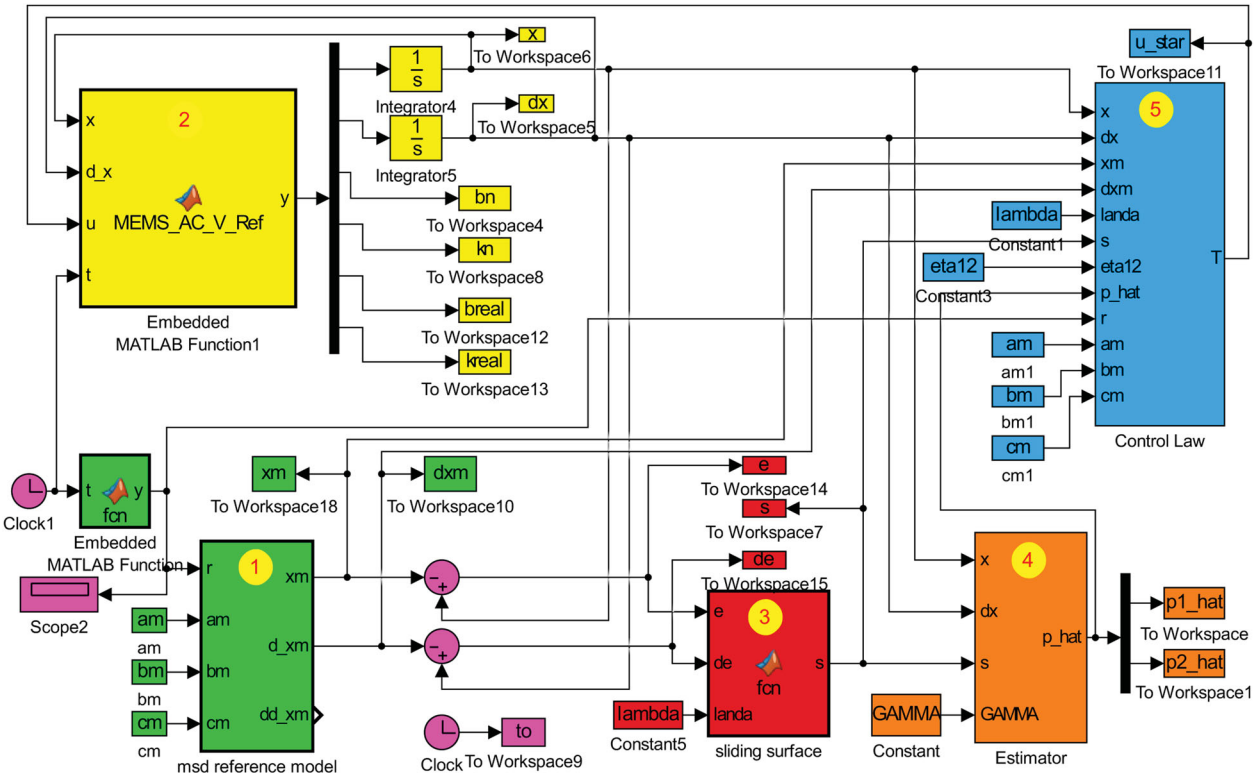

Figure 4. Simulation scheme of the conventional ASMC design. It is notable that no disturbance is imposed on the ASMC, testifying the system under less exacerbated condition in comparison with the RASMC.

Table 3. Blocks in the simulation scheme of the ASMC and their corresponding implementation equations.

Block No.	Equation No.	Block No.	Equation No.	Block No.	Equation No.	Block No.	Equation No.	Block No.	Equation No.
1	(15)	2	(14) and (13)	3	(87)	4	(92)	5	(89)

uncertainties, in particular at the conventional ASMC design, has tremendously impressed its tracking performance destructively, preventing the moveable plate from reaching its convenient pull-in point.

The simulation of the old ASMC design is done being subjected to the same uncertainties but less exacerbating condition – without any disturbance imposed on the system. However, comparing Figure 5(a,b) with Figure 5(c,d), respectively, notifies one of the great difference in tracking performance of the two proposed methods. The conventional ASMC is quite incapable of providing the required accuracy in the moveable plate placement at the pull-in point. The system shows an oscillatory behaviour around the steady-state point causing the real system even to be unstable in practice. Moreover, it should not be concealed out of mind that the design basics in the ASMC, contrary to the new RASMC, has not taken into account the uncertainty in the moveable plate mass. However, the novel RASMC design shows considerably greater robustness and accuracy in tracking the desired trajectory of $x_m(t)$ instead, suggesting preference over the old ASMC.

Both the RASMC design and ASMC apply similar switching function such as sat(.) in the structure of their control laws. The subtle point is that when the stiffness and damping coefficients in their system dynamics are subjected to rapid variation, described by Equations (94) and (95), the RASMC show greater robustness against parameter variation in comparison with ASMC. Figure 5(a,b) are representative of the simulation results for RASMC and Figure 5(c,d) display simulation yields for ASMC, respectively. As seen on Figure 5(a,b), the RASMC design is not affected by variation of the parameters in the tracking task while the ASMC system, as displayed on Figure 5(c,d), suffers from variation of the parameters since the plate displacement in Figure 5(c) or the error in Figure 5(d) is quite affected by the noise (parameter variation).

5. Conclusion

The MEMS tunable capacitors are considered as the main components of the AC VRS. The movable plate in this tunable capacitor ought to be steered towards the pull-in point achieving the desired output voltage. The possible time-dependant uncertainties existing in the system dynamics of the tunable capacitor bring about difficulty in obtaining non-destructive perfect displacement tracking of the moveable plate towards the final pull-in settling point, exploiting the conventional ASMC. Although numerous efforts are done to modify fabrication process in order to manufacture

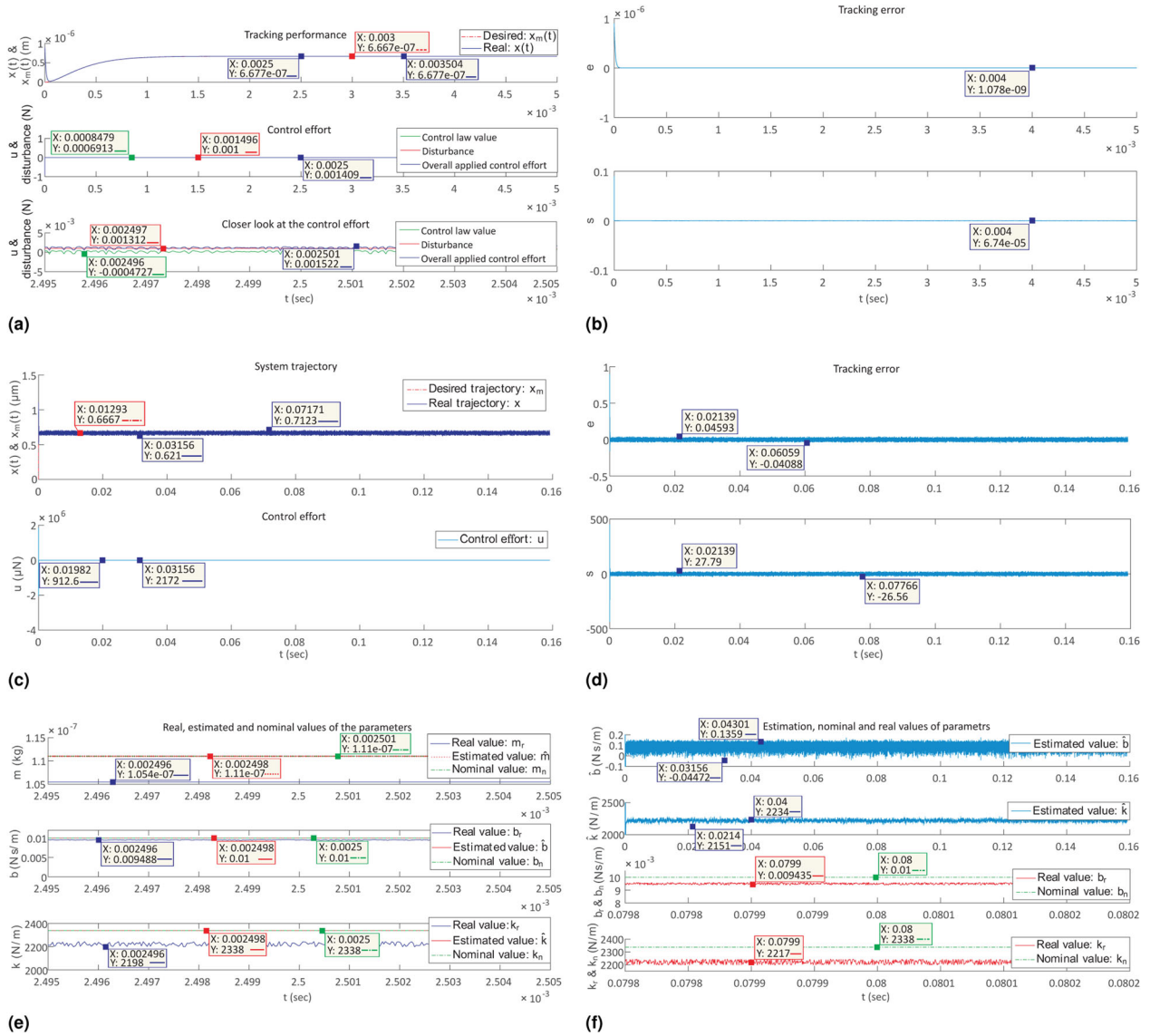

Figure 5. Tracking performance in the novel RASMC design based on dead-zone technique (a and b) in the conventional ASMC. (c and d) Estimation of parameters versus their real values at the dead-zone-based RASMC (e) and ASMC (f).

the MEMS tunable capacitor with the desired physical specification, the static uncertainties as well as dynamic intrinsic electromechanical ones unavoidably transpire in the MEMS device such as the time-invariant mass ambivalence or the bounded time-variant stiffness and damping uncertainties. The proposed dead-zone-based robust ASMC is capable of faultless tracking of desired position trajectory of the movable plate in the existence of the parametric uncertainties, exogenous disturbance as well as lumped nonlinearities. The tracking error in the RASMC is approximately zero and is about 1.078×10^{-9} ($\Delta e \simeq 0$) while the error is changing from -0.041 to 0.046 in the previous ASMC design ($\Delta e \simeq 0.005$) for the specified simulation time interval. Actually, one may notice that the position of the plate is changing from 0.621 to 0.7123 μm in the steady state. In other words, the displacement error has reduced about 100% ($\frac{1.078\times10^{-9}-0.046}{0.046} \simeq -0.999$). Consequently, the desired output voltage is generated by the AC VRS. The whole controlling scheme owns the advantage of disturbance rejection in comparison to the old ASMC; it also demonstrates noticeable robustness against aggravating disturbance enforced on the system and the time-variant changes in the parameter values.

6. Discussion and research prospective

Drawing the article big picture, one issue which requires one's prospective attention is parameter identification working along side the adaptive controller to estimate the stiffness and damping factors for catalogue purposes. The other is designing and tuning a fuzzy ASMC to bring more robustness to the controller. Investigation of its possible landmark effect over rejection of disturbance and reduction of voltage noise floor could be deemed as other upcoming research field. Some works have contributed to address parametric uncertainties and external disturbance via usage of robust adaptive controller; however, it mandates one to

think about design of a controller which comprehensively and simultaneously tackles numerous issues such as measurement noise, disturbance, parameter variation and the control effort energy consumption.

A sophisticated integrated simulation should be adopted to verify the efficiency of our proposed controller from the implementation aspect. For instance, the capacitive displaceable plate should be modelled as a dynamical system in Comsol. On the other side, the controller is simulated in Matlab Simulink. Then, the former and the latter simulated models should be connected in real-time. Now, significant mechanical analyses such as tension analysis, displacement analysis, deformation modal investigation, and spectrum analysis of the control effort signal could be carried out. It leads to more implementation evaluation of the suggested controller and investigation of adverse frequency components in the control effort signal.

Introducing a dead zone using Equation (86) means that no adaption takes place in the nearby vicinity of the sliding manifold. In this zone, the adaption law is not updated. This actually indicates that the adaption law is not performing well as error goes to zero. Although one may troubleshoot the problem tuning Δ_d, a better law could be designed which makes the adapted coefficient converge continuously since we have limitation on the reduction of dead-zone band.

Disclosure statement

No potential conflict of interest was reported by the authors.

ORCID

Ehsan Ranjbar http://orcid.org/0000-0002-1759-1236

References

[1] Suhonen M, Seppa H, Oja AAC and DC voltage standards based on silicon micromechanics. Conference on Precision Electromagnetic Measurements Digest; 1998. p. 23–24. doi:10.1109/CPEM.1998.699739

[2] Kärkkäinen A, Pesonen N, Suhonen M, et al. AC voltage reference based on a capacitive micromechanical component. Conference on Precision Electromagnetic Measurements Digest; 2004. p. 119–120. doi:10.1109/CPEM.2004.305489

[3] Kärkkäinen A, Pekko P, Dekker J, et al. Stable SOI micromachined electrostatic AC voltage reference. Microsyst Technol. 2005;12(1–2):169–172. doi:10.1007/s00542-005-0005-y

[4] Blard F, Bounouh A, Bélières D, et al. Very high stability achievement in MEMS based AC voltage references. IEEE 24th International Conference on Micro Electro Mechanical Systems (MEMS); 2011. p. 656–659. doi:10.1109/MEMSYS.2011.5734510

[5] Bounouh A, Camon H, Bélières D, et al. MEMS AC voltage reference for miniaturized instrumentation and metrology. Comput Stand Interfaces. 2011;33(2):159–164. doi:10.1016/j.csi.2010.06.007. XVI IMEKO TC4 "Symposium Exploring New Frontiers of Instrumentation and Methods for Electrical and Electronic Measurements" and XIII International Workshop on ADC Modelling and Testing.

[6] Bounouh A, Camon H, Belieres D. MEMS based AC voltage references with very high stability. Conference on Precision Electromagnetic Measurements (CPEM); 2012. p. 552–553. doi:10.1109/CPEM.2012.6251048

[7] Bounouh A, Camon H, Belieres D. Wideband high stability MEMS-Based AC voltage references. IEEE Trans Instrum Meas. 2013;62(6):1646–1651. doi:10.1109/TIM.2012.2225963

[8] Kärkkäinen A, Oja A, Kyynäräinen J, et al. Stability of electrostatic actuation of MEMS. Physica Scripta. 2004;2004(T114):193. doi:10.1088/0031-8949/2004/T114/048

[9] Barhaghtalab MH, Bayani H, Nabaei A, et al. On the design of the robust neuro-adaptive controller for cable-driven parallel robots. Automatika. 2016;57(3):724–735. doi:10.7305/automatika.2017.02.1793

[10] Fei J, Batur C. A novel adaptive sliding mode control with application to MEMS gyroscope. ISA Trans. 2009;48(1):73–78. doi:10.1016/j.isatra.2008.10.008

[11] Ranjbar E, Suratgar AA. A composite adaptive controller design for 3-DOF MEMS vibratory gyroscopes capable of measuring angular velocity. Iran J Sci Technol Trans Electr Eng. 2018;43(2):245–266. doi:10.1007/s40998-018-0101-5

[12] Ranjbar E, Suratgar AA. Design of a composite adaptive controller for the single-axis 2-DOF MEMS vibratory gyroscope with the competency of rotation rate measurement. Control Eng Appl Inform J (CEAI). 2018;20(3).

[13] Fei J. Robust adaptive vibration tracking control for a micro-electro-mechanical systems vibratory gyroscope with bound estimation. IET Control Theory Appl. 2010;4(6):1019–1026. doi:10.1049/iet-cta.2008.0199

[14] Hassane FA, Payam AF, Fathipour M. Design of a smart MEMS accelerometer using nonlinear control principles. Smart Struct Syst. 2010;6(1):1–16. doi:10.12989/sss.2010.6.1.001

[15] Fei J, Xin M, Juan W. Adaptive fuzzy sliding mode control using adaptive sliding gain for MEMS gyroscope. Trans Inst Measur Control. 2013;35(4):551–558. doi:10.1177/0142331212455451

[16] Juan W, Fei J. Adaptive fuzzy approach for non-linearity compensation in MEMS gyroscope. Trans Inst Measur Control. 2013;35(8):1008–1015. doi:10.1177/0142331212472224

[17] Wu D, Fei J. Adaptive neural sliding control of MEMS gyroscope with robust feedback compensator. Trans Inst Measur Control. 2016;38(4):414–424. doi:10.1177/0142331215585879

[18] Modirrousta A, Shokrian Zeini M, Binazadeh T. Nonlinear optimal fuzzy control synthesis for robust output tracking of uncertain micro-electro-mechanical systems; 2016. doi:10.1177/0142331216630363

[19] Fei J, Batur CA. class of adaptive sliding mode controller with proportional-integral sliding surface. Proc Inst Mech Engin Part I J Syst Control Engin. 2009;223(7):989–999. doi:10.1243/09596518JSCE712

[20] Liu D, Li PM. Adaptive wavelet neural network backstepping sliding mode tracking control for pmsm drive system. Automatika. 2014;55(4):405–415. doi:10.7305/automatika.2014.12.456

[21] Nafia N, Kari AE, Ayad H, et al. A robust type-2 fuzzy sliding mode controller for disturbed mimo nonlinear systems with unknown dynamics. Automatika.

2018;59(2):194–207. doi:10.1080/00051144.2018.1521568

[22] Feng J, Gao Q, Guan W, et al. Fuzzy sliding mode control for erection mechanism with unmodelled dynamics. Automatika. 2017;58(2):131–140. doi:10.1080/00051144.2017.1377913

[23] Mehrnezhad A, Suratgar A, Khatami S, et al. A mathematical dynamic model for static and dynamic behaviours of MEMS-based AC voltage reference source. 21st Iranian Conference on Electrical Engineering (ICEE); 2013. p. 1–5. doi:10.1109/IranianCEE.2013.6599714

[24] Ranjbar E, Mehrnezhad A, Suratgar AA. Adaptive sliding mode control of MEMS AC voltage reference source. J Control Sci Eng. 2017;2017:14. doi:10.1155/2017/9425190

[25] Fei J, editor. Advanced control design of MEMS vibratory gyroscope. New York (NY): Nova Science Publishers; 2012.

[26] Lhee C-G, Park J-S, Ahn H-S, et al. Sliding mode-like fuzzy logic control with self-tuning the dead zone parameters. IEEE Trans Fuzzy Syst. 2001;9(2):343–348. doi:10.1109/91.919255

[27] Ranjbar E, Suratgar AA, Kabganian M. Design of an adaptive controller for a 2-DOF MEMS vibratory gyroscope to obtain perfect tracking and angular velocity estimation with noise, disturbance and parameter variation analysis. The 3rd International Conference on Control, Instrumentation, and Automation; 2013. p. 224–23. doi:10.1109/ICCIAutom.2013.6912839

[28] Ranjbar E, Suratgar AA. Design of a quadratic linear tracking controller to minimize battery power consumption of a 2-DOF MEMS vibratory gyroscope. The 3rd International Conference on Control, Instrumentation, and Automation; 2013. p. 198–202. doi:10.1109/ICCIAutom.2013.6912834

[29] Farzanegan B, Niafar E, Ranjbar E, et al. Two MRAC designs for the MEMS-based AC voltage reference source. Iran J Sci Technol Trans Electr Eng. 2019;43(4):773–784. doi:10.1007/s40998-019-00205-7

[30] Ranjbar E, Yaghoubi M, Suratgar AA. Adaptive sliding mode controller design for a tunable capacitor susceptible to unknown upper-bounded uncertainties and disturbance. Iran J Sci Technol Trans Electr Eng. 2019;44(1):327–346. doi:10.1007/s40998-019-00220-8

[31] Batur C, Sreeramreddy T, Khasawneh Q. Sliding mode control of a simulated MEMS gyroscope. ISA Trans. 2006;45(1):99–108. doi:10.1016/S0019-0578(07)60069-X

[32] Fei J, Wu D. Adaptive control of MEMS gyroscope using fully tuned RBF neural network. Neural Comput Appl. 2015;28(4):695–702. doi:10.1007/s00521-015-2098-2

[33] Ranjbar E, Suratgar A. Compensation for cross-coupling error in a 2-DOF MEMS vibratory gyroscope via designing a state feedback controller. 3rd International Conference on Acoustics & Vibration (ISAV2013); 2013 Dec 25–26; Tehran, Iran. 2013.

[34] Chu Y, Fang Y, Fei J. Adaptive neural dynamic global pid sliding mode control for mems gyroscope. Int J Mach Learn Cyber. 2016;8(5):1707–1718. doi:10.1007/s13042-016-0543-x

[35] Ranjbar E, Shahbazi M, Suratgar A. Designing a state feedback controller to compensate for quadrature error in a 3-DOF MEMS vibratory gyroscope. 4th International Conference on Acoustics and Vibration (ISAV2014); 2014 Dec 10–11, Tehran, Iran. 2014.

[36] Yang Y, Fei J. Adaptive sliding mode control of mems gyroscope based on neural network approximation. J Appl Math. 2014;2014:159047. doi:10.1155/2014/159047

[37] Ren J, Zhang R, Xu B. Adaptive fuzzy sliding mode control of mems gyroscope with finite time convergence. J Sensors. 2016;2016:1572303. doi:10.1155/2016/1572303

[38] Ranjbar E, Mehrnezhad A, Suratgar A, et al. Adaptive control of MEMS-based AC voltage reference source. 22nd Iranian Conference on Electrical Engineering (ICEE); 2014. p. 1336–1341. doi:10.1109/IranianCEE.2014.6999741

[39] Ranjbar E, Suratgar AA. Design of an adaptive sliding mode controller with a sliding mode luenberger observer for the MEMS capacitive plates. SN Appl Sci. 2020;2(3):351. doi:10.1007/s42452-020-2148-y

[40] Castñer L, Pons J, Nadal-Guardia R, et al. Analysis of the extended operation range of electrostatic actuators by current-pulse drive. Sens Actuators A Phys. 2001;90(3):181–190. doi:10.1016/S0924-4247(01)00525-8

[41] Kärkkäinen AM. MEMS based voltage references [PhD Thesis]. Espoo: VTT Technical Research Centre of Finland; 2006. Dissertation for the degree of Doctor of Philosophy to be presented with due permission of the Department of Electrical and Communications Engineering for public examination and debate in the Large Seminar Hall of Micronova at Helsinki University of Technology.

[42] Slotine J, Li W. Applied nonlinear control. Englewood Cliffs (NJ): Prentice Hall; 1991. ISBN 9780130408907.

[43] Liu X, Jiang W, Dong XC. Nonlinear adaptive control for dynamic and dead-zone uncertainties in robotic systems. Int J Control Autom Syst. 2017;15(2):875–882. doi:10.1007/s12555-015-0449-5